Adv Syst Sci Appl 2022; **01**:15–34

Published online at https://ijassa.ipu.ru.

Direct Torque Control-Fuzzy Type 2 for Direct Current Link Voltages Balancing of the Five-Level Cascade Converters Used in a Wind Energy Conversion System

Abdelhafidh Moualdia[1*], Saleh Boulkhrachef[1], Patrice Wira[2]

[1]*LREA Laboratory, Faculty of Technology, University of Medea, Ain d'heb Medea, Algeria*

[2]*IRIMAS Laboratory, University of Haute Alsace, Mulhouse, France*

Abstract: The available power of a wind system depends mainly on the wind speed. In addition, the wind system will give a power output that varies according to the speed of its generator which is a double feed asynchronous machine in our case. In other words, there is an optimal operating point that makes the most of the power available. In this work an innovative technique of capturing maximum power based on type-2 fuzzy systems. The principle of this Maximum Power Point Tracking algorithm is to look for an optimal operating relationship at maximum power and then track the maximum power based on this relationship. As part of the variable speed conversion of wind energy, this article proposes a simplified power electronics for injecting the energy produced in the network, the conversion chain includes a variable speed double feed asynchronous generator, two (back-to-back) converters five-level Neutral Point Clamped type operating in grid side rectifier and rotor-side inverter mode. The main objective of this article is to develop a new stabilization strategy of direct control compatible with voltage inverters at five levels, more particularly Neutral Point Clamped structure. This strategy allows flow and torque control of the double feed asynchronous machine and stabilizes the input capacitor voltages of the inverter. The response of the system obtained with this algorithm makes it possible to validate the soft solution proposed and show, during variation of the wind speed, a fast and precise adaptation of the speed of the double fed induction generator.

Keywords: double fed induction generator, direct current link voltage, fuzzy type 2, direct torque control, wind energy, five level converter cascade

1. INTRODUCTION

From a general point of view, regardless of the topology, multilevel conversion structures offer huge advantages over a conventional solution, based on a two-level converter [1, 2]. These advantages are visible, on the one hand from a technological point of view and on the other hand from a functional point of view. First of all, the quality of the output signal of the inverter can be improved thanks to the additional degree of freedom which is the number of voltage level [3–6]. The switched voltage is of reduced amplitude and the switching is therefore easier to manage. Despite the advantages of multi-level inverters, the instability of capacitor voltages on the DC side remains the major disadvantage of multi-level NPC (Neutral Point Clamped) inverters [7, 8].
As a result, the imbalance of these voltages leads to the failure of power components and deformation of the output voltage. For this, several solutions are proposed. These solutions include methods based on vector modulation techniques, where the concept of redundant

*Corresponding author: amoualdia@gmail.com

voltage vectors has been applied to balance the electrical charge between capacitors [9–11]. However, for high levels, the number of voltage vectors increases considerably and thus the control becomes complex. Other solutions, based on the addition of auxiliary circuits for the balancing of these DC voltages of the inverter, are proposed in the literature .
To be able to replace the DC drive and enjoy the advantages of the asynchronous motor, the control must be more and more efficient. DTC (Direct Torque Control) control strategy has emerged as competitive with vector control techniques. This DTC command was invented by I. Takahashi in the $mid - 1980s$. It is based on the separate regulation of the rotor flux and the electromagnetic torque of the double-feed asynchronous generator. In order to provide better control of NPC-structured five-level inverter voltages and achieve better performance, the wind energy conversion system is connected to the power grid using rectifiers controlled by the width modulation. Pulse (PWM). These rectifiers can provide a low harmonic distortion in the input currents, a grid-side adjustable power factor, and a constant DC output voltage. Control of rectifiers based on fuzzy systems is also possible [12]. In particular, the fuzzy controller methodology appears useful when information sources are considered unclear or uncertain.
In an ordinary fuzzy system, the membership functions, once determined, are completely precise, and therefore unable to take into account the uncertainty of the linguistic terms used in the premises and consequences of the rules. To solve this limitation, the fuzzy set type-2 was introduced as an extension of the fuzzy set type-1, where each degree of membership of each element is itself a fuzzy set in [0, 1]. [13–15]. First, we first present a description of the DFIG-based wind energy conversion system. The second part of this work will be dedicated to the synthesis of innovative technique of maximum power capture based on type-2 fuzzy systems. The principle of this Maximum Power Point Tracking (MPPT) algorithm is to look for an optimal operating relationship at maximum power and then track the maximum power based on this relationship. In the third step, the development of a stabilizing DTC control, to

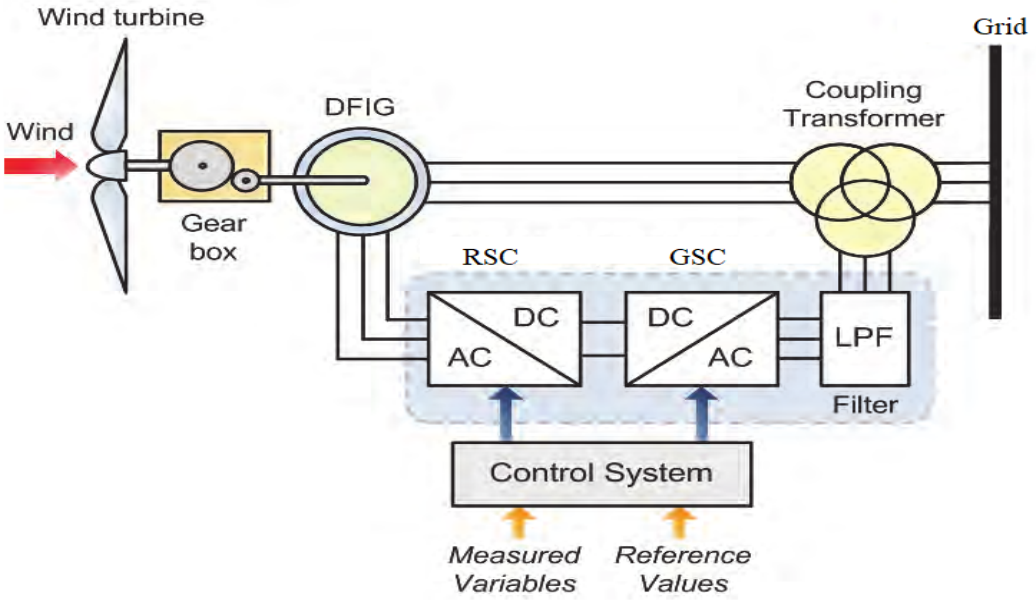

Fig. 1.1. Wind energy conversion system based on five-level NPC cascaded converters

solve the problem of the imbalance of the input voltages of the 5-level converter with NPC structure on the rotor side. Taking advantage of the redundancies of the state of the rotor side converter, producing the same voltage vector, but opposite effects on the voltages of the capacitors, an algorithm is developed. This allows us to balance the capacitor voltages in addition to controlling the torque and flux of the double feed asynchronous generator. The

wind energy conversion system description based on five-level NPC cascaded converters is shown in Figure 1.1.

NOMENCLATURE

β	blade pitch angle;
$\mathbf{V}$	wind speed (m/s);
ρ	air density;
λ	speed ratio;
$\mathbf{C_p}$	power coefficient;
$\mathbf{P_m}$	mechanical power (kW);
$\mathbf{T_m}$	mechanical Torque ;
$\mathbf{V_{sdq}}, V_{rdq}$	dq axis stator and rotor voltages ;
$\mathbf{i_{sdq}}, i_{rdq},$	dq axis stator and rotor current ;
$\omega_\mathbf{s}, \omega_r,$	stator and rotor pulsation (rd/s) ;
$\mathbf{\Phi_{sdq}}, \Phi_{rdq},$	dq axis stator and rotor flux ;
$\mathbf{M},$	mutual inductance ;
$\mathbf{P_s}, Q_s$	generator active and reactive powers ;
$\mathbf{P_1}, \mathbf{P_2}$	logical function ;
$\mathbf{J}, f$	moment of inertia and coefficient of friction ;
$\mathbf{E_1}, \mathbf{E_2}, \mathbf{E_3}$	load conditions ;
$\mathbf{k}$	Phase number (k=1, 2, 3);
$\mathbf{C_1}; \mathbf{C_2}; \mathbf{C_3}; \mathbf{C_4}$	DC-link capacitors;
$\mathbf{U_{C1}}; \mathbf{U_{C2}}; \mathbf{U_{C3}}; \mathbf{U_{C4}}$	DC bus voltages;
$\mathbf{I_{C1}}; \mathbf{I_{C2}}; \mathbf{I_{C3}}; \mathbf{I_{C4}}$	Capacitors currents;
$\mathbf{I_{rec1}}; \mathbf{I_{rec2}}; \mathbf{I_{rec3}}; \mathbf{I_{rec4}}$	Output rectifier currents;
$\mathbf{I_{netk}^{ref}}$	Reference network phase current;
$\mathbf{I_{rec}^{ref}}$	Reference network phase current;
$\mathbf{V_{sk}}; \mathbf{i_{sk}}$	Stator phase voltage and current;
$\mathbf{V_{s\alpha\beta}}, \mathbf{i_{s\alpha\beta}}$	Stator voltage and current in the stationary $\alpha - \beta$ plane
$\mathbf{\Omega}, \mathbf{\Omega_n}$	Rotor speed and speed nominal value;
$\mathbf{T_{em}}, \mathbf{T_{ref}}$	Electromagnetic torque and reference value;
$\mathbf{\Phi_s}$	Stator flux magnitude;
$\mathbf{\Phi_{s\alpha}}, \mathbf{\Phi_{s\beta}}$	Stator flux magnitude in $\alpha - \beta$ plane
$\mathbf{f_{net}}$	Network frequency;
$\mathbf{V_{Di}}$	Discrete voltage level of vector V_s;
$\mathbf{C_{fl}}$	Output Hysteresis flux controller;
$\mathbf{C_{tr}}$	Output Hysteresis Torque controller;

ABBREVIATIONS USED

NPC :	Neutral Point Clamped	HVDC :	high voltage direct current
DC :	Direct Current	DTC :	Direct Torque Control
PWM :	Pulse Width Modulation	CSR :	Current Source Rectifier
IM :	Induction machine	SVM :	Space-Vector Modulation
FLC :	Fuzzy Logic Controller	T1FLS :	Type-1 Fuzzy Sets
T2FLS :	Type-2 Fuzzy Sets	PI :	Proportional Integral Controller
DFIG :	Double Fed Induction Generator	MPPT :	Maximum Power Point Tracking
RSC :	rotor-side Converter	GSC :	Grid-side Converter

2. DESCRIPTION OF THE WIND CONVERSION SYSTEM

2.1. *Wind turbine model*

The mechanical power available on the shaft of a wind turbine can be expressed as [22, 26]:

$$P_m = 0.5C_p\left(\lambda\right)\pi\rho R^2 V_1^3, \tag{2.1}$$

For the variables speed wind turbines, approximate expression of the power coefficient can be described by the following expression:

$$\begin{aligned} C_p f\left(\lambda,\beta\right) = C_1\left(\frac{C_2}{\lambda_i} - C_3 - C_4\right)\exp\left(\frac{-C_5}{\lambda_i}\right) \\ +C_6\lambda, \end{aligned} \tag{2.2}$$

Where:

$$\frac{1}{\lambda_i} = \frac{1}{\lambda + 0.08\beta} - \frac{0.035}{\beta^3 + 1} \tag{2.3}$$

Where, $C_1 = 0.5176, C_2 = 116, C_3 = 0.4, C_4 = 5, C_5 = 21, C_6 = 0.0068$.The torque produced by the turbine is expressed in the following way:

$$T_m = \frac{P_m}{\Omega_m} = \left(0.5\pi\rho R^3 V_1^2\right)\frac{C_p(\lambda,\beta))}{\lambda} \tag{2.4}$$

No wind turbine could convert more than 59 of the kinetic energy of the wind into mechanical energy turning the rotor [16]. This is known as the Betz limit and it's the C_{pmax} theoretical maximum coefficient of power (for any wind turbine): $C_{pmax} = 16/27 \approx 0.593$. In practice, for the good turbines it's in the range of 0.45 to about 0.50. The tip speed ratio (λ) for wind

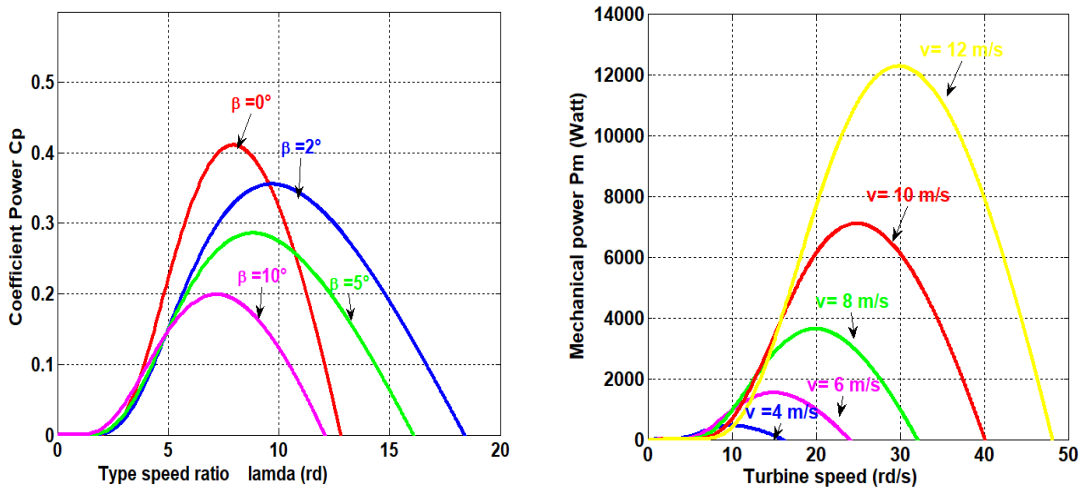

(a) (b)

Fig. 2.2. (a): for Pitch angle effect on the aerodynamic coefficient of power and (b): for mechanical power output.

turbines is the ratio between the rotational speed of the tip of a blade and the actual velocity of the wind, see Figure 2.2.

Table 2.1. Inference matrix

de\e	NG	NM	NP	EZ	PP	PM	PG
NG	NG	NG	NM	NM	NP	NP	EZ
NM	NG	NM	NM	NM	NP	EZ	PP
NP	NG	NM	NP	NP	EZ	PP	PM
EZ	NG	NM	NP	EZ	PP	PM	PG
PP	NM	NP	EZ	PP	PP	PM	PG
PM	NP	EZ	PP	PM	PM	PM	PG
PG	EZ	PP	PP	PM	PG	PG	PG

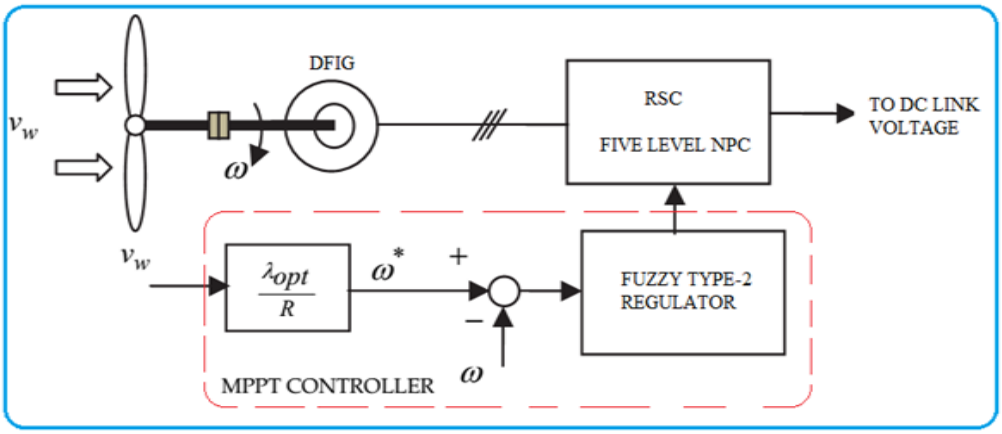

Fig. 2.3. Tip speed ratio control (MPPT).

2.2. Maximum power tracking via fuzzy-type 2 systems

At a given wind speed, the maximum turbine energy conversion efficiency occurs at an optimal TSR Figure 2.3. Therefore, as wind speed changes the turbine's rotor speed needs to change accordingly in order to maintain the optimal tip speed ratio TSR and thus to extract the maximum power from the available wind resources.

The structure of the fuzzy type-2 regulator is shown in Figure 2.4. In order to have the desired performances, the normalization gains at the input and at the output of the regulator are determined by adjustment. For input and output variables consisting of seven fuzzy sets type-2 interval, the conventional anti-diagonal inference matrix of a fuzzy system is given in Table 2.1.

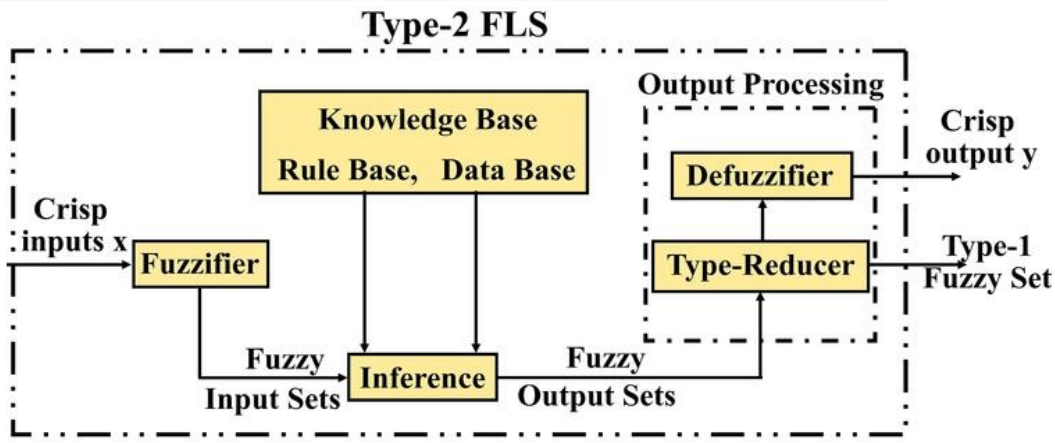

Fig. 2.4. Structure of the fuzzy type-2 controller.

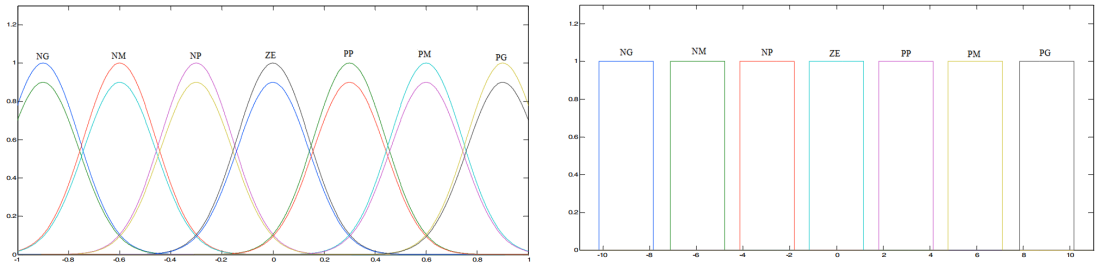

(a) (b)

Fig. 2.5. membership functions.(a):membership functions of input variables,(b):membership functions of output variables

2.3. Modelling of the double fed induction generator

In the rotating field reference frame of Park, the model of the DFIG is given by the following equations [30, 31]:

$$\begin{aligned} V_{sd} &= R_s i_{sd} + \tfrac{d}{dt}\Phi_{sd} - \omega_s \Phi_{sq} \\ V_{sq} &= R_s i_{sq} + \tfrac{d}{dt}\Phi_{sq} + \omega_s \Phi_{sd} \\ V_{rd} &= R_r i_{rd} + \tfrac{d}{dt}\Phi_{rd} - \omega_r \Phi_{rq} \\ V_{rq} &= R_r i_{rq} + \tfrac{d}{dt}\Phi_{rq} + \omega_r \Phi_{rd}, \end{aligned} \tag{2.5}$$

Stator and rotor voltages components:

$$\begin{aligned} \Phi_{sd} &= L_s i_{sd} + M i_{rd} \\ \Phi_{sq} &= L_s i_{sq} + M i_{rq} \\ \Phi_{rd} &= L_r i_{rd} + M i_{sd} \\ \Phi_{rq} &= L_r i_{rq} + M i_{sq}. \end{aligned} \tag{2.6}$$

Double fed induction generator electromagnetic torque:

$$C_{em} = C_r + J\frac{d\Omega}{dt} + f\Omega, \tag{2.7}$$

Generator active and reactive powers at the grid side are:

$$\begin{cases} P_s = V_{sd}i_{sd} + V_{sq}i_{sq} \\ Q_s = V_{sq}i_{sd} - V_{sd}i_{sq}. \end{cases} \tag{2.8}$$

2.4. Five-Level NPC converter

Multilevel converters are power-conversion systems composed by an array of power semiconductors and capacitive voltage sources that, when properly connected and controlled, can generate a multiple-step voltage waveform with variable and controllable frequency, phase, and amplitude. The stepped waveform is synthesized by selecting different voltage levels. The numbers of levels of a converter is defined as the number of steps that can be generated by the converter between the output terminal and any reference node within the converter, is usually denoted by N and called neutral. To be called a multilevel converter, each phase of the converter has to generate at least three different voltage levels. This differentiates the classic tw o-level voltage source converter $(2L - VSC)$ from the multilevel family.
The neutral clamped inverter, also known as diode clamped inverter. The basic architecture of this inverter discussed in references [17, 18]. The neutral clamped inverter obtained the

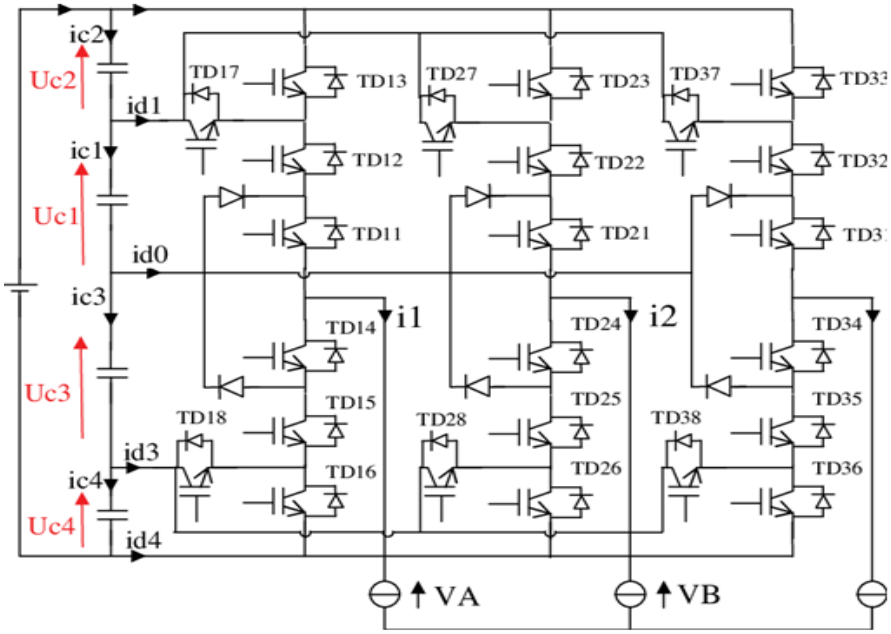

Fig. 2.6. The Five-Level NPC converter.

staircase output voltage. If m is the number of level, then the number of capacitors required on the DC bus are (m -1), the number of power electronic switches per phase are 2(m -1) and the number of diodes per phase are $2(m-2)$. The DC bus voltage has three levels using two capacitors C_1 and C_2, for five levels using four capacitors C_1, C_2, C_3 and C_4 as shown in Figure 2.6. Table 2.2 lists the voltage levels and their corresponding switch states. State 1 means that the switch is on, and 0 means that the switch is off. We suppose that all the DC voltage sources are the same and equal to nominal value . The output voltage vector is defined

Table 2.2. Switching states and output voltage of the first leg of the five-level NPC inverter

State	V_{1M}	S_{11}	S_{12}	S_{13}	S_{14}	S_{15}	S_{16}	S_{17}	S_{18}
+2	$+2U_c$	1	1	1	0	0	0	0	0
+1	$+U_c$	1	1	0	0	0	1	1	0
0	0	1	0	0	1	0	0	0	0
-1	$-U_c$	0	0	1	1	1	0	0	1
-2	$-2U_c$	0	0	0	1	1	1	0	0

as:

$$\begin{aligned} V_s &= V_{aM}e^{j0} + V_{bM}e^{-j2\pi/3} + V_{cM}e^{-j4\pi/3} \\ &= V_\alpha + jV_\beta. \end{aligned} \tag{2.9}$$

It can be observed that 24 vectors can be generated by a unique switching state, 18 vectors can be generated using two switching states each (2 redundancy), 12 vectors can be generated using three switching states each (3 redundancies), 6 vectors can be generated using four switching states each (4redundancies), and one vector can be generated using five switching states (5redundancies). [15, 16]

3. DTC FOR FIVE-LEVEL ROTOR SIDE CONVERTER (RSC)

In recent years, a new control strategy based on direct control of flux and torque has been proposed. This technique, known as DTC, enables the induction motor to deliver a very quick and accurate torque response.The instantaneous values of flux and torque are calculated from measured variables (voltages and currents) and then controlled directly by selecting optimum inverter switching modes.The objective of this section is to present the DTC of induction machine fed by a five–level NPC inverter. The schematic diagram of the proposed DTC system is shown in Figure 3.7. As in the original DTC principle the $\alpha - \beta$ plane will be divided into several sectors [26]. In a five-level inverter the number of discrete voltage vectors is more important than those obtained with a two-level inverter.
Thus, the $\alpha - \beta$ plane will be divided into 12 sectors rather than six. At each one of these sectors, an appropriate voltage vector will be assigned to keep flux and torque references as needed.The speed of the stator flux vector is given by the modulus of the applied space voltage vector. Thus, the space voltage vectors will be chosen according to the rotor speed. Voltage vectors with low amplitude will be chosen for low speeds, and vectors with greater amplitude will be chosen for higher speeds. In the five-level inverter, four tables have been used, according to a specific speed range, as shown in Table 2.2 . Three different states are used to identify torque status and two states for flux.

4. CONTROL STRATEGY OF THE BALANCING CAPACITOR VOLTAGE

We will present the proposed DTC algorithm to balance DC bus voltages using redundant configurations of the five-level inverter. The, each discrete voltage level can be obtained by more than one switching state. As the voltage evolution for a given capacitor will be different for each state, this redundancy let's to control the capacitors voltages while the requested space vector voltage is supplied. Based on this property, a control strategy will be

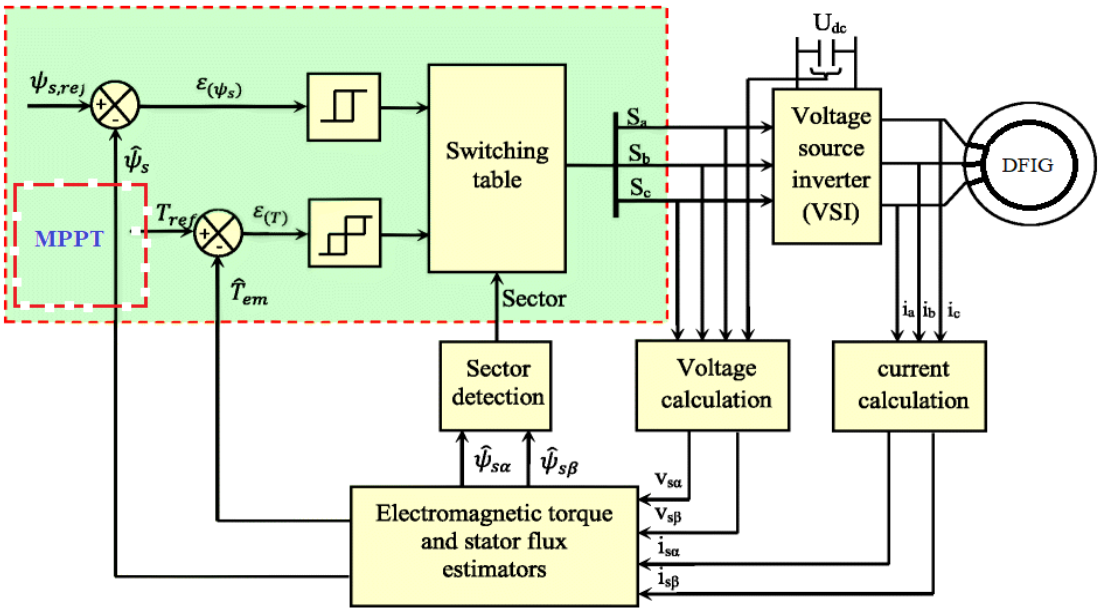

Fig. 3.7. Schematic diagram of the proposed DTC system.

Table 4.3. Six groups of redundant vectors

Group 1	V_{p1}	V_{p4}	V_{p7}	V_{p10}	V_{p13}	V_{p16}
Group 2	V_{p2}	V_{p6}	V_{p8}	V_{p12}	V_{p14}	V_{p18}
Group 3	V_{p3}	V_{p5}	V_{p9}	V_{p11}	V_{p15}	V_{p17}
Group 4	V_{p19}	V_{p21}	V_{p23}	V_{p25}	V_{p27}	V_{p29}
Group 5	V_{p20}	V_{p22}	V_{p24}	V_{p26}	V_{p28}	V_{p30}
Group 6	V_{p31}	V_{p32}	V_{p33}	V_{p34}	V_{p35}	V_{p36}

presented and applied to a five-level inverter. To do so, we firstly study the effect of different redundant vectors on capacitor voltages. In Table 5.4, all the redundant vectors of the space vector diagram and the corresponding capacitors currents according to the load (i1, i2, i3) are presented. Depending on the forms of relationships (Equation 2.9, 4.10 and 4.11 in Table 4.3), we distinguish six groups of redundant vectors:

4.1. Effect of redundant vectors on capacitor voltages

Redundant vectors of each group can increase or decrease capacitor voltages, depending on load conditions sign of (Equation 2.9, 4.10 and 4.11. For groups with one Equation 2.9 (groups 1, 4 and 6), we have two possibilities of load conditions, each one is associated with a logical function:

$$\begin{aligned} P_1 &= 1 \; if \; E_1 > 0 \; else \; P_1 = 0 \\ P_2 &= 1 \; if \; E_1 \leq 0 \; else \; P_2 = 0. \end{aligned} \tag{4.10}$$

For groups with three (Equation 2.9, 4.10 (groups 2, 3 and 5), we have six possibilities of load conditions, associated with six logical functions:

$$\begin{aligned}
&P_1 = 1\ if\ E_1 < 0, E_2 < 0, and\ E_3 > 0, else\ P_1 = 0;\\
&P_2 = 1\ if\ E_1 < 0, E_2 > 0, and\ E_3 < 0, else\ P_2 = 0;\\
&P_3 = 1\ if\ E_1 < 0, E_2 > 0, and\ E_3 > 0, else\ P_3 = 0;\\
&P_4 = 1\ if\ E_1 > 0, E_2 < 0, and\ E_3 < 0, else\ P_4 = 0;\\
&P_5 = 1\ if\ E_1 > 0, E_2 < 0, and\ E_3 > 0, else\ P_5 = 0;\\
&P_6 = 1\ if\ E_1 > 0, E_2 > 0, and\ E_3 < 0, else\ P_6 = 0.
\end{aligned} \tag{4.11}$$

4.2. Choice of redundancies

For each case of redundancy, the vector which reduces the fluctuation voltages in capacitors will be selected. The diagram of the control algorithm is shown in Figure 4.8. We select the vector which charge the undercharged capacitors, and discharge the overcharged ones. To do so, we must measure capacitor voltages and calculate their deviation case. Each deviation case is characterized by a logical function Cj (Table 5.4.). For example, the first case : $U_{c1} < U_{c2} < U_{c3} < U_{c4}$ is associated to the function C_1, defined as: For each group of redundancies, given the deviation case (C_j). And load state (P_i), the vector that will decrease the largest capacitor voltage and increase the smallest capacitor voltage is selected. In Table 5.4, the choice of redundancies (a, b, c, d) according to the load states and capacitor voltages deviation case is presented.

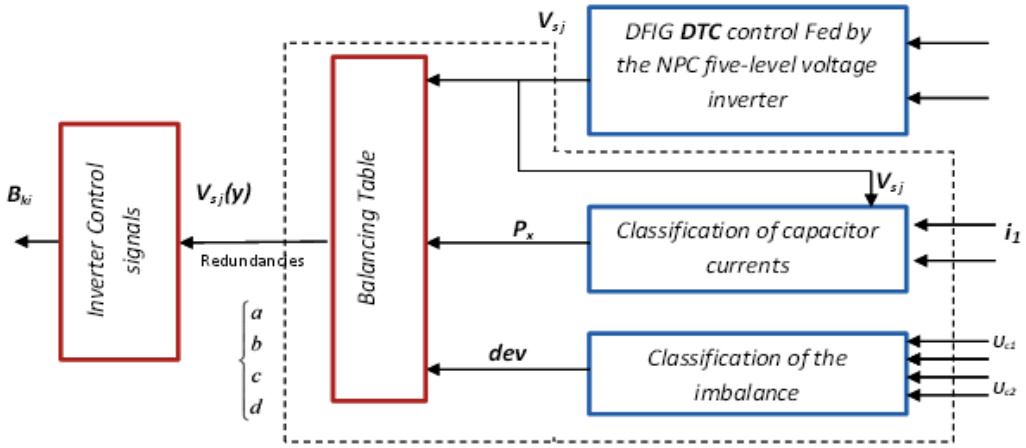

Fig. 4.8. Capacitor voltages balancing algorithm

5. CONTROL OF FIVE-LEVEL GRID SIDE CONVERTER (GSC)

In this section, a current control strategy of three-phase five-level PWM rectifier applying a type-2 fuzzy system is proposed. Figure 5.10 shows the schematic of the control of the 5-level rectifier. This block diagram is based on the control of the average value of the output voltages, using a type-2 fuzzy controller. The purpose of servo-control is to determine the network reference currents applied to the hysteresis comparators. This control is done with a

unit power factor, requiring zero reactive power, if imposing a zero phase shift between the voltage and current per phase of the power grid. By Hysteresis current control, the switching of the transistors ensures that the input phase currents track the reference currents within the tolerance band. The three-phase reference currents are given by the following expressions:

$$i_{ref} = \sqrt{2} I_{reg} \sin\left(\omega t - \varphi - (j-1)\tfrac{2\pi}{3}\right); \quad j = 1, 2, 3 \tag{5.12}$$

φ is the desired phase shift given to the currents with respect to the corresponding voltages. In our case, φ is set to zero for unity power factor operation.

5.1. Type-2 Fuzzy Logic Controller Design

Figure 5.9 depicts the structure of a type-2 FLC. It is quite similar to a type-1 FLC. The major difference being that at least, one of the fuzzy sets are type-2 and a type-reducer is needed to convert the output of the fuzzy inference engine into type-1 fuzzy set called type-reduce set. These type-reduced set is defuzzified to obtain the crisp output $dIreg$. Throughout of

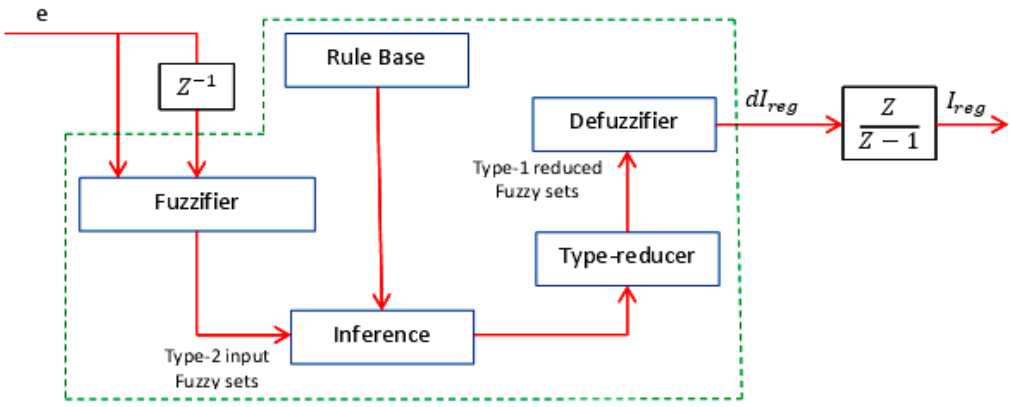

Fig. 5.9. Structure of a T2 FLC

this paper, an interval typ2 FLC with singleton input fuzzification is considered. Indeed, the Interval type-2 fuzzy sets are simple to use and can simplify effectively the computational process of type-reduction.
The controller output $dIreg$ is calculated by the T2FLC of Figure 5.9, which uses the rule base of Table 2.1. This table is commonly used to construct fuzzy controller. The next step is to construct the fuzzy rules for processing the fuzzy input. Assume that there are M rules in the type-2 fuzzy system, where the ith rule has the following form:

$$R^i : if\ e\ is\ \widetilde{F_{de}^i}\ then\ dI_{reg}\ is\ \widetilde{G^i} = [u_l^i, u_r^i]; i = 1, ..., M. \tag{5.13}$$

Where $\widetilde{F_e^i}$ and $\widetilde{F_{de}^i}$ are antecedent linguistic terms modelled by the interval type-2 triangular fuzzy sets, dI_{reg} is the output and the consequent term G^i is an interval type-1 set which can be called weighting interval set $[u_l^i, u_r^i]$. u_l^i and u_r^i are the singleton lower and upper control actions of the consequent part.

Table 5.4. Selection of redundancies

	Groups	**1**		**2**						**3**						**4**		**5**						**6**	
C_j	**load state** $P_i\backslash\backslash$ **states capacitors voltages**	P_1	P_2	P_1	P_2	P_3	P_4	P_5	P_6	P_1	P_2	P_3	P_4	P_5	P_6	P_1	P_2	P_1	P_2	P_3	P_4	P_5	P_6	P_1	P_2
1	$U_{c2} < U_{c1} < U_{c3} < U_{c4}$	a	b	b	a	b	a	b	a	b	a	b	a	b	a	a	c	c	a	c	a	c	a	d	a
2	$U_{c2} < U_{c1} < U_{c4} < U_{c3}$	a	b	b	b	b	a	a	a	b	a	b	a	b	a	a	c	c	a	c	a	b	a	c	a
3	$U_{c2} < U_{c3} < U_{c1} < U_{c4}$	a	b	b	a	b	a	b	a	b	a	b	a	b	a	a	c	c	b	b	a	c	a	d	a
4	$U_{c2} < U_{c3} < U_{c4} < U_{c1}$	a	b	b	a	b	a	b	a	b	b	b	a	a	a	a	b	b	b	b	a	a	a	b	a
5	$U_{c2} < U_{c4} < U_{c1} < U_{c3}$	a	b	b	b	b	a	a	a	b	b	b	a	a	a	a	b	b	c	c	a	b	a	c	a
6	$U_{c2} < U_{c4} < U_{c3} < U_{c1}$	a	b	b	b	b	a	a	a	b	b	b	a	a	a	a	b	b	c	b	a	a	a	b	a
7	$U_{c1} < U_{c2} < U_{c3} < U_{c4}$	a	b	b	a	b	a	b	a	b	a	a	b	b	a	a	c	c	a	c	b	c	a	d	b
8	$U_{c1} < U_{c2} < U_{c4} < U_{c3}$	a	b	b	b	b	a	a	a	b	a	a	b	b	a	a	c	c	a	c	b	b	a	c	b
9	$U_{c1} < U_{c3} < U_{c2} < U_{c4}$	a	b	b	a	a	b	b	a	b	a	a	b	b	a	b	c	c	a	a	b	c	b	d	b
10	$U_{c1} < U_{c3} < U_{c4} < U_{c2}$	b	a	a	a	a	b	b	b	a	a	a	b	b	b	b	c	c	a	a	b	c	b	a	b
11	$U_{c1} < U_{c4} < U_{c2} < U_{c3}$	b	a	a	b	b	a	a	b	a	a	a	b	b	b	a	c	c	a	c	b	b	a	c	b
12	$U_{c1} < U_{c4} < U_{c3} < U_{c2}$	b	a	a	b	a	b	a	b	a	a	a	b	b	b	b	c	c	a	a	b	b	b	a	b
13	$U_{c3} < U_{c2} < U_{c1} < U_{c4}$	a	b	b	a	a	b	b	a	b	a	b	a	b	a	b	a	a	b	b	c	c	b	d	c
14	$U_{c3} < U_{c2} < U_{c4} < U_{c1}$	a	b	b	a	a	b	b	a	b	b	b	a	a	a	c	a	a	b	b	c	a	c	b	c
15	$U_{c3} < U_{c1} < U_{c2} < U_{c4}$	a	b	b	a	a	b	b	a	b	a	a	b	b	a	b	a	a	b	a	c	c	b	d	c
16	$U_{c3} < U_{c1} < U_{c4} < U_{c2}$	b	a	a	a	a	b	b	b	a	a	a	b	b	b	b	a	a	b	a	c	c	b	a	c
17	$U_{c3} < U_{c4} < U_{c2} < U_{c1}$	b	a	a	a	a	b	b	b	a	b	b	a	a	b	c	a	a	b	b	c	a	c	b	c
18	$U_{c3} < U_{c1} < U_{c4} < U_{c2}$	b	a	a	a	a	b	b	b	a	b	a	b	a	b	b	a	a	b	a	c	a	c	a	c
19	$U_{c3} < U_{c4} < U_{c1} < U_{c2}$	b	a	a	b	b	a	a	b	a	b	b	a	a	b	c	b	b	c	c	a	b	c	c	d
20	$U_{c4} < U_{c2} < U_{c3} < U_{c1}$	b	a	a	b	b	a	a	b	a	b	b	a	a	b	c	b	b	c	b	a	a	c	b	d
21	$U_{c4} < U_{c1} < U_{c2} < U_{c3}$	b	a	a	b	b	a	a	b	a	b	a	b	a	b	c	b	b	c	c	b	b	c	c	d
22	$U_{c4} < U_{c1} < U_{c3} < U_{c2}$	b	a	a	b	a	b	a	b	a	b	a	b	a	b	c	a	a	c	a	b	b	c	a	d
23	$U_{c4} < U_{c3} < U_{c2} < U_{c1}$	b	a	a	b	a	b	a	b	a	b	b	a	a	b	c	a	a	c	b	c	a	c	b	d
24	$U_{c4} < U_{c3} < U_{c1} < U_{c2}$	b	a	a	b	a	b	a	b	a	b	a	b	a	b	c	a	a	c	a	c	a	c	a	d

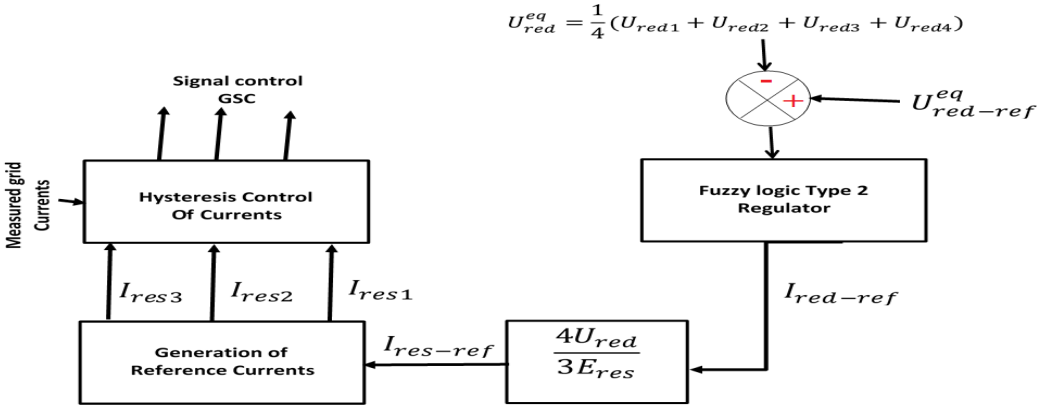

Fig. 5.10. Grid side five levels NPC converter control

The inference engine combines the fuzzy rules in order to map the crisp inputs to interval type-2 fuzzy output sets. Based on the input and the antecedents of the rules, it calculates a firing interval for each rule and then applies these firing levels to the consequent fuzzy sets. The firing interval $[\underline{F^i}, \overline{F^i}]$ of the i^th rule is an interval type-1 set, which is determined by its left-most and right-most points $\underline{F^i}$ and $\overline{F^i}$ such that :

$$\overline{F^i} = \min\left(\underline{\mu}_{\widetilde{F_e^i}}(e), \underline{\mu}_{\widetilde{F_e^i}}(de)\right) \tag{5.14}$$

$$\overline{F^i} = \min\left(\overline{\mu}_{\widetilde{F_e^i}}(e), \overline{\mu}_{\widetilde{F_e^i}}(de)\right) \tag{5.15}$$

Where $\underline{\mu}_{\widetilde{F_e^i}}(x)$ and $\overline{\mu}_{\widetilde{F_e^i}}(x)$ represent the grade of the lower and the upper membership function of the crisp input x to the type-2 fuzzy set $\widetilde{F_x^i}$ in i^th rule. The output corresponding to the fired rule is a type-2 fuzzy set which must be type-reduced before the Defuzzifier can be used to generate a crisp output. There are several methods for type reduction, such as center-of-sums type-reduction, height type-reduction, modified height type-reduction, and center-of-sets type-reduction. In this paper, the centre-of-sets type-reducer is used which can be represented by $dI_{ref} = \left[dI_{refl}^i, dI_{refr}^i\right]$.The output is an interval type-1 set. Therefore, we only need to compute its two endpoints dI_{refl}^i and dI_{refr}^i as follows:

$$dI_{refl} = \frac{\sum_{i=1}^{M} F_l^i u_l^i}{\sum_{i=1}^{M} F_l^i} \tag{5.16}$$

$$dI_{refr} = \frac{\sum_{i=1}^{M} F_r^i u_r^i}{\sum_{i=1}^{M} F_r^i} \tag{5.17}$$

In order to compute dI_{ref}, we need to compute dI_{refl} and dI_{refr} . This can be done using the procedure given in [25], [26]. Without loss of generality, assume that the pre-computed u_r^i are arranged in ascending order,i.e.$u_r^1 \leq u_r^2 \leq ..... \leq u_r^M$

- step 1 : Compute dI_{refr} in Equation 5.17 by initially setting $F_r^i = \frac{\left(\underline{F^i} + \overline{F^i}\right)}{2}$, for $i = 1, 2, ..., M$ where $\underline{F^i}$ and $\overline{F^i}$ have been computed using Equation 5.15 respectively,and let $dI_{refr}{}' = dI_{refr}$.
- step 2 : Find $k\,(1 \leq k \leq M-1)$ such that $u_r^k \leq dI_{refr}{}' \leq u_r^{(k+1)}$.

- step 3 : Compute dI_{ref} in Equation 5.17 with $F_r^i = \underline{F^i}$ for $i \leq k$ and $F_r^i = \overline{F^i}$ for $i > k$, then set ${dI_{refr}}'' = dI_{refr}$.
- step 4 :If ${dI_{refr}}'' \neq {dI_{refr}}'$, then go to step 5. If ${dI_{refr}}'' = {dI_{refr}}'$ then set $dI_{refr} = {dI_{refr}}''$ and go to step 6.
- step 5 :set ${dI_{refr}}' = {dI_{refr}}''$ and return to step 2.
- step 6 : End

The procedure for computing dI_{refl} is very similar, only two changes need to be made: In step 2, we need to find $k\,(1 \leq k' \leq M-1)$ such that $u_l^m \leq {dI_{refl}}' \leq u_l^m$, m=k'+1 and in step 3, let $F_l^i = \overline{F^i}$ for $i \leq k'$ and $F_l^i = \underline{F^i}$ for $i > k'$. From the type-reduction stage, we have for each output a type-reduced set. The crisp output of the type-2 fuzzy controller can be obtained by using the average value of dI_{refr} and dI_{refl} . Hence, the defuzzified crisp output becomes:

$$dI_{refk} = \frac{dI_{refkl} + dI_{refkr}}{2} \tag{5.18}$$

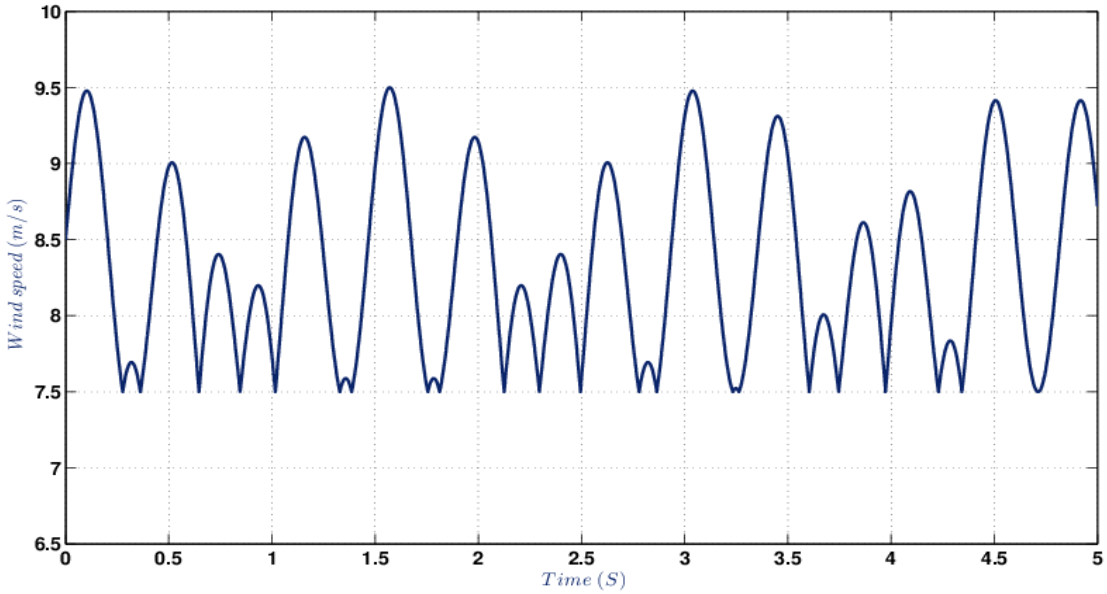

Fig. 5.11. Wind speed profile

6. SIMULATION RESULTS

In order to demonstrate the feasibility of the proposed control method, simulation testing are undertaken on the structure shown in Figure 1.1. The most commonly encountered disturbances in drive applications are changes in the load torque or changes in the speed. It is important thereby to show if the proposed cascade is able to handle aforementioned transients and ensure the stability of DC-bus voltages.

The wind speed profile applied to energy conversion system is shown with in Figure 5.11. The multilevel DTC strategy has been tested by simulation in different level of speed control loop.The reference speed is obtained by the MPPT block. The control objective in this section is to show the performance in both interest operation regions (I and III) of the turbine characteristic. In the region III, one can see that the stator power is limited at its

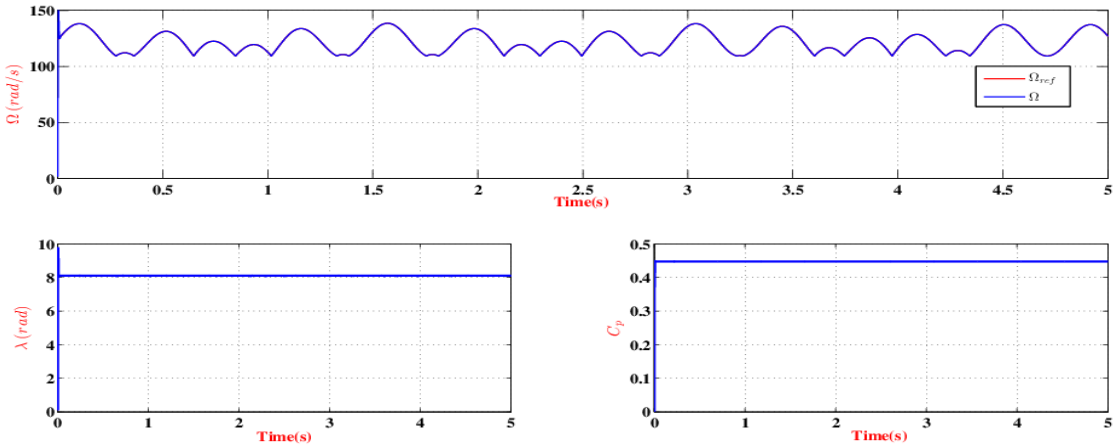

Fig. 6.12. MPPT result

maximum value by the pitch angle control,as shows Figure 6.12. This is approved by the waveforms illustrated in Figure 6.17 of the tip speed ratio (λ) and the power coefficient (C_p). The mechanical speed is kept constant, at its limit value, as plotted in Figure 6.12.

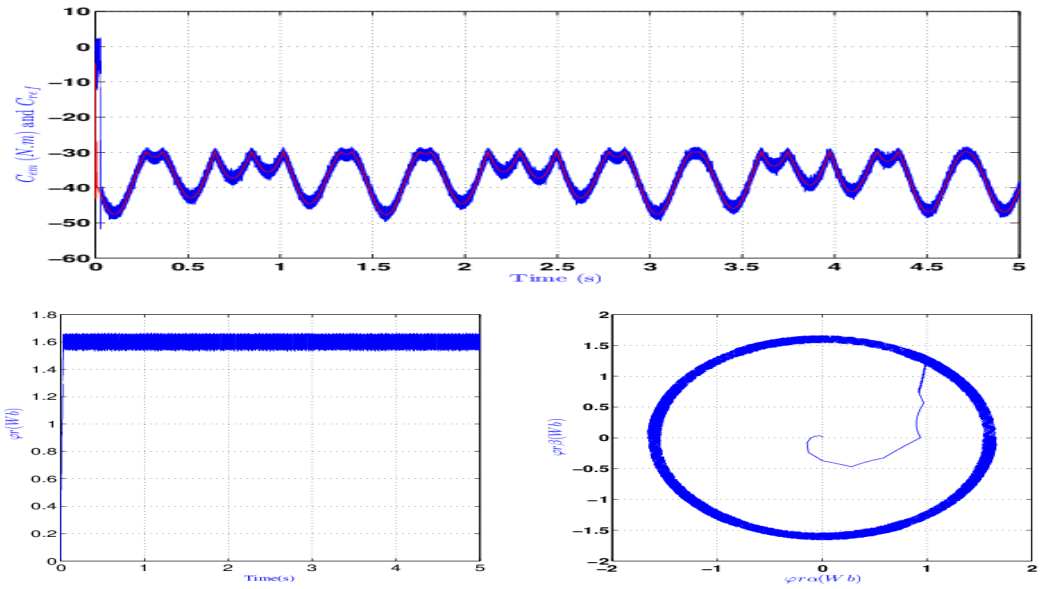

Fig. 6.13. Response of electromagnetic torque and rotor flux

However, in region I the power is maximized by the MPPT algorithm. In this case, as expected, tip speed ratio and the power coefficient are maintained at constant values see Figure 6.12 ($\beta = 0$,$\lambda = \lambda_{opt} = 8.1$, $C_p = C_{p-max} = 0.49$). The reference tracking reflecting the robustness of the proposed control under random behavior of wind speed. Figure 6.13 shows the rotor flux waveform, it is circular and kept constant at 1.6 Wb. The random evolution of the rotor current magnitude is related to the electromagnetic torque variations and their pulsation is depending on the slip variations. The operation as a generator is illustrated by the negative sign of the electromagnetic torque $C_{em} < 0$, with a variable amplitude, which depends on the wind speed evolution, as presented in Figure 6.13 where we can see that the operation with constant power is clear within the over-speed zone. In Figure 6.14, the

capacitor voltages with the proposed DTC balancing strategy are shown .
It can be seen that the balancing of the capacitor voltages is achieved sufficiently over the full speed state and for all load torque of induction machine, which prove that the stability of DC voltages with proposed strategy is independent of machine operating points. In the study-state condition, the maximum of each capacitor voltage ripple is less than $4\text{V}\ (2\%)$, which shows the effectiveness of the DTC balancing strategy. Consequently, the different between the voltages capacitor tends to zero, as shown in Figure 6.15.

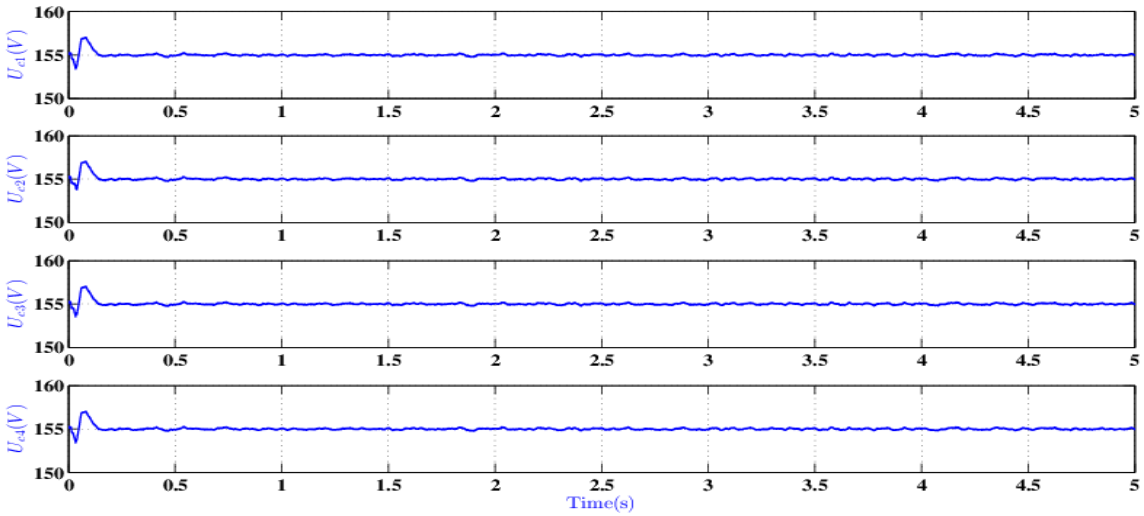

Fig. 6.14. Response of DC-link voltages with proposed DTC control strategy.

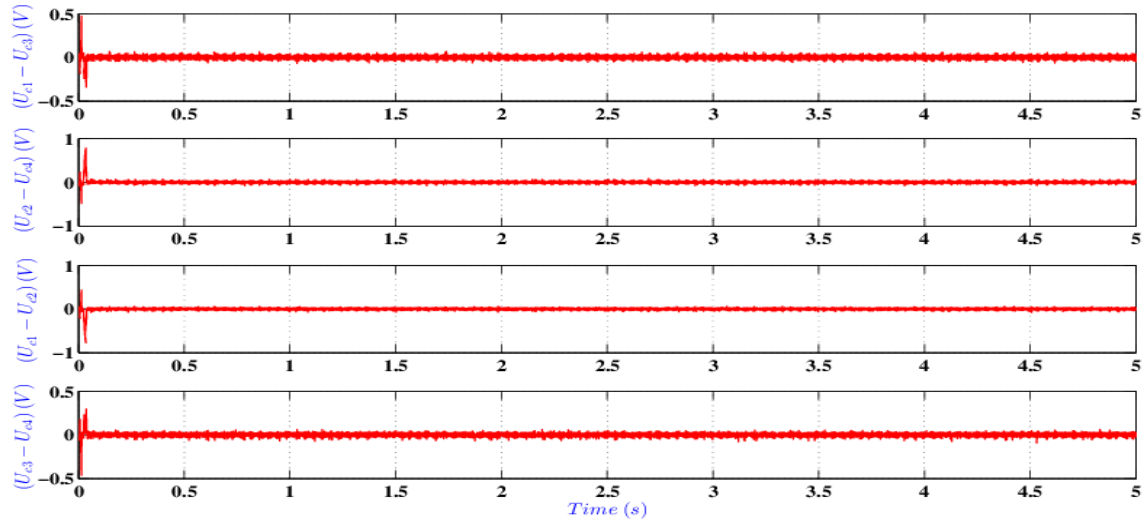

Fig. 6.15. Error DC-link voltages.

7. CONCLUSION

In this work, the application of direct torque control in a wind energy conversion system supplied by a five level NPC back-to-back converter has been presented. The choice of this

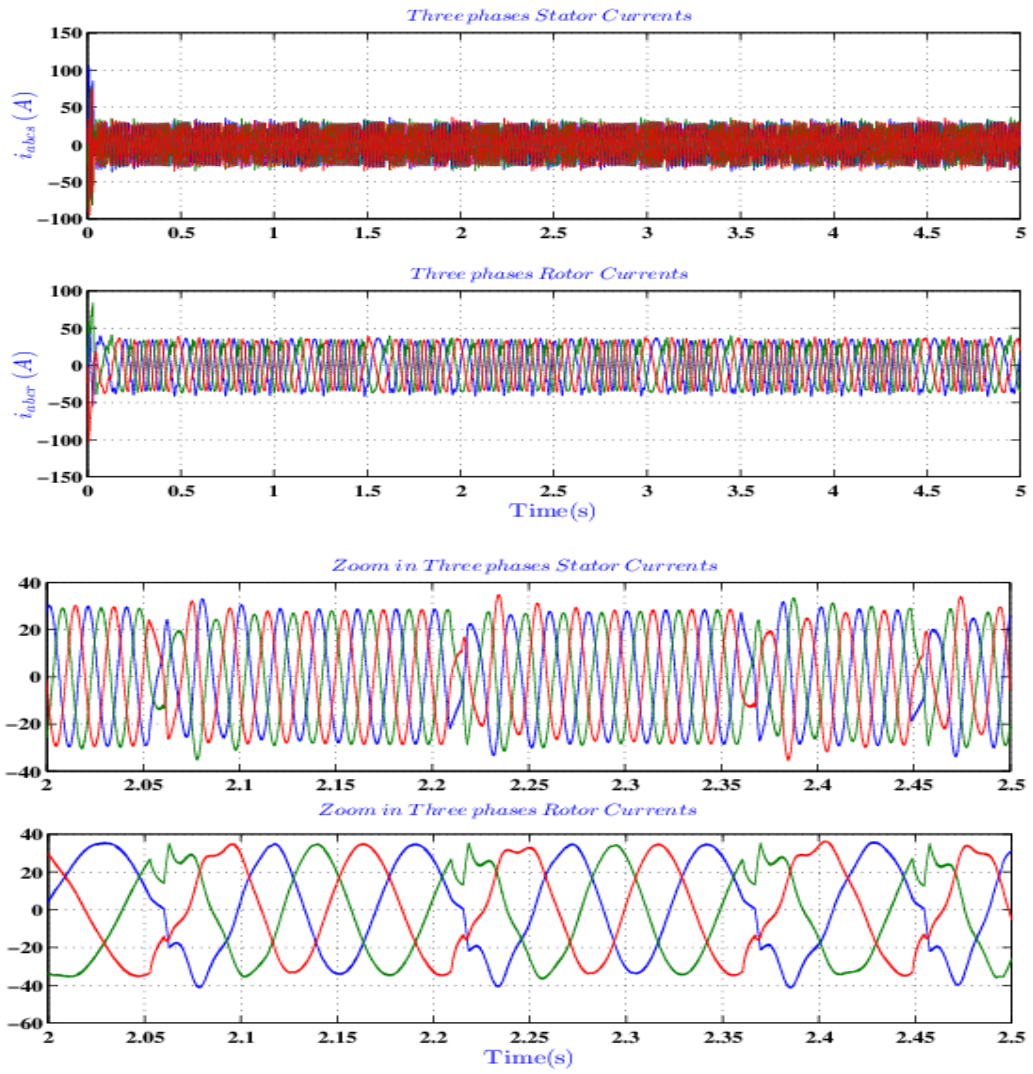

Fig. 6.16. Response of stator and rotor currents

structure allows a bidirectional flow of power, and provides regeneration capability.Another advantage of the back-to-back system is that it can control easily the input power factor. The effectiveness of the proposed DTC-based voltage balancing strategy it demonstrated under various operating conditions of double fed induction generator. Is may therefore be concluded that the proposed multilevel direct torque control not only has the advantage of reducing the undesirable torque ripple, but also has the additional advantage of preventing the voltage drift phenomen on of the DC-link capacitors of the back-to-back system, longer life of DC-link capacitors can be achieved. Furthermore, the employment of multilevel topology improves the stator voltage quality, reducing electromagnetic interference and isolation stress problems of windings. This results in the reduction of radiated emissions, which makes this kind of drives a less polluting system than the traditional two-level drive. In addition, this study has successfully demonstrated the application of type-2 fuzzy systems to control the DC-link voltage, and the maximization of power tracking. It found that the type-2 fuzzy control scheme could achieve good performance in terms of overshoot, steady-state error, torque disturbance, and variable speed tracking.

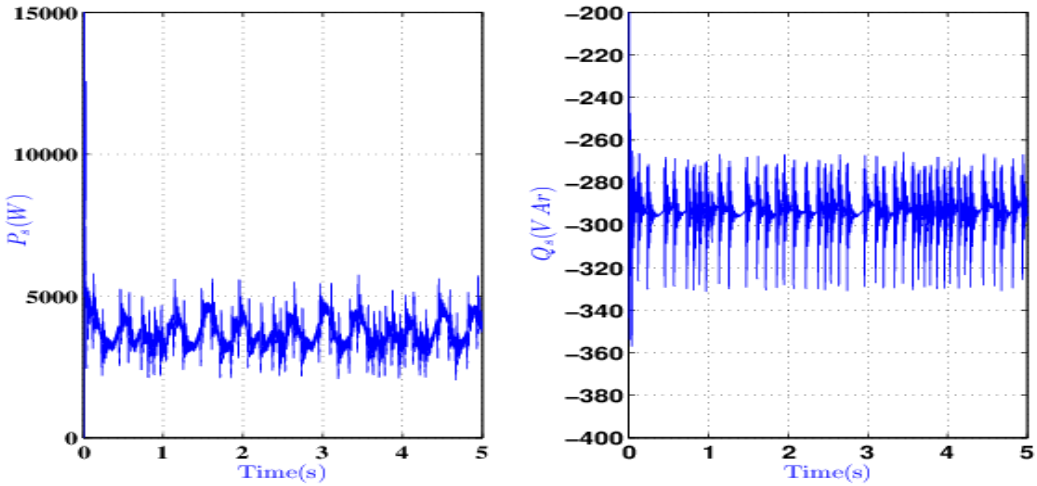

Fig. 6.17. Response of stator active and reactive power

ACKNOWLEDGEMENTS

The research is part of a project PRFU'2020, realized respectively in the laboratory of electrical engineering and automatic LREA research, University of Medea, and IRIMAS Laboratory, University of Haute Alsace, Mulhouse, France.

REFERENCES

1. Polinder, H., F. F. A. Van Der Pijl, G. J.de Vilder and P. J. (2006) Tavner.Comparison of Direct-Drive and Geared Generator Concepts for Wind Turbines. *IEEE Transactions on Energy Conversion.*, **21** (3), 725–733.
2. P.Liutanakul , A.Awan, S.Pierfederici, B.Nahid-Mobarakeh , F. M.Tabar.(2010) Linear Stabilization of a DC Bus Supplying a Constant Power Load: A General Design Approach. *IEEE Transactions on Power Electronics*, **22** (2),475–488.
3. X.Sun , Y.Tian , Z.Chen. (2014) Adaptive decoupled power control method for inverter connected DG. *IET Renewable Power Generation*, **8** (2),171–182.
4. Brabandere, K, Bolsens, B., Keybus, J. Woyte, A. Driesen, J. Belmans, R.(2007) A voltage and frequency droop control method for parallel inverters. *IEEE Trans. Power Electron*, **22** (4),1107–1115.
5. Wang, Y., X. Wang and D. Gerling.A.(2018) Precise Voltage Distortion Compensation Strategy for Voltage Source Inverters. *IEEE Transactions on Industrial Electronics.*, **65** (1) 59–66.
6. Vovos, N. A., P. N. Vovos and K. G.Georgakas.(2014) Harmonic Reduction Method for a Single-Phase DC-AC Converter without an OutputFilter. *IEEE Transactions on Power Electronics.*, **29** (9), 4624–4632.
7. Kapoor, P. and M. Renge.(2017) Improved Performance of Modular Multilevel Converter for Induction Motor Drive. *Energy Procedia.*, **117** (1),361–368.
8. G.c. Diyoke, C.U.Ogbuka, C.M.Nwosu. (2019) A Novel Control DC-DC-AC Buck Converter for Single Phase Capacitor-Start-Run Induction Motor Drives. *power engineering and electrical engineering*,**17** (2),87–95.
9. Ajami, A., H. Ardi and A. Farakhor.(2014) Design,Analysis and Implementation of a Buck-Boost DC/DC Converter. *IET Power Electronics.*, **7** (12),2902–2913.
10. Bartman, J.(2017) Analysis of Output Voltage Distortion of Inverter for Frequency Lower than Nominal. *Journal of Electrical Engineering.* **68** (3),194–199.

11. Hanafy, H. (2014) Dynamic Analysis of a New Connection for Dual Voltage Operation of Single Phase Capacitor Run Motor. *Journal of Electrical Engineering.*, **13** (1),1–8.
12. Ojaghi, M. and S. Daliri.(2017) Analytic Model for Performance Study and Computer-Aided Design of Single-Phase Shaded-Pole Induction Motors.*IEEE Transactions on Energy Conversion.*, **32** (2),649–657.
13. Leon, J. I., S. Vazquez and L. G. Franquelo. (2017) Multilevel Converters: Control and Modulation Techniques for their Operation, *Industrial Applications. Proceedings of the IEEE.*, **105** (11),2066–2081.
14. Franquelo, L., J. Rodriguez, J. Leon, S. Kouro, R. Portillo and M. Prats.(2007) The Age of Multilevel Converters Arrives. *IEEE Industrial Electronics Magazine.*, **2** (2) ,28–39.
15. Babaei, E., S. Laali and S. Bahravar.(2015) A New Cascaded Multi-level Inverter Topology with Reduced Number of Components and Charge Balance Control Methods Capabilities.*Electric Power Components and Systems*, **43** (19) ,2116–2130.
16. Kimball, J. and M. Zawodniok. (2011) Reducing Common-Mode Voltage in Three-Phase Sine-Triangle PWM with Interleaved Carriers. *IEEE Transactions on Power Electronics.* **26** (8),2229–2236.
17. Mohamad R. Banaei, M. R. Jannati Oskuee and F. Mohajel Kazemi.NA. (2014) New Advanced Topology of Stacked Multicell Inverter. *International Journal of Emerging Electric Power Systems*, **15** (4),327–333.
18. Sadigh Ak, Hosseini Sh, Sabahi M, Gharehpetian Gb.(2010) Double flying capacitor multicell converter based on modified phase-shifted pulsewidth modulation.*IEEE Trans Power Electron*, **25** (6),1517–1526.
19. W. Fengxiang, C. Zhe, P. Stolze, J.-F. Stumper, J. Rodriguez, R. Kennel. (2014) Encoderless finite-state predictive torque control for induction machine with a compensated MRAS.*IEEE Trans. Ind. Informat*, **10** (2),1097–1106.
20. Wang, L., M. Zhao, X. Wu, X. Gong and L. Yang. Fully. (2017) integrated high-efficiency high step-down ratio DC–DC buck converter with predictive over-current protection scheme. *IET Power Electronics*, **10** (14),1959–1965.
21. H.Kouki, M.Fredj, B. Rehaoulia. (2016) Harmonic analysis of SVPWM control strategy on VSI-fed double-star induction machine performances, *Electrical Engineering*,**98** (2),133–143.
22. A.Ziaei, R.Ghazi, R.Z.Davarani.(2018) Linear Modal Analysis of Doubly-Fed Induction Generator (DFIG) Torsional Interaction: Effect of DFIG Controllers and System Parameters,*Advances in Electrical and Electronic Engineering* ,**16** (4),388 – 401.
23. Zhu, C., L. Fan and M. Hu. (2010) Control and analysis of DFIG-based wind turbines in a series compensated network for SSR damping.*In: IEEE PES General Meeting. Michigan:* IEEE, 1–6.
24. Van, T. L., T. D. Ngyen, T. T. Tran and H. D. Nguyen.(2015) Advanced Control Strategy of Back-to-Back PWM Converters in PMSG Wind Power System. *Advances in Electrical and Electronic Engineering*, **12** (2),81–95.
25. Leon, A. E. and J. A. Solsona. (2015) Sub-Synchronous Interaction Damping Control for DFIG Wind Turbines. *IEEE Transactions on Power Systems*, **30** (1),419–428.
26. T.Vaimann, O.Kudrjavtsev, A.Kilk, A.Kallaste, A.Rassolkin. (2018) Design and Prototyping of Directly Driven Outer Rotor Permanent Magnet Generator for Small Scale Wind Turbines.*Advances in Electrical and Electronic Engineering*, **16** (3),271–278.
27. Boulkhrachef, S., Berkouk, E. M., Barkat, S. Benkhoris, M. F. (2012) Self Voltage Balancing for the Five Level Back to Back Converter using Multilevel DTC and Type-2 Fuzzy Logic Controller. The Mediterranean Journal of Measurement and Control,**8** (4),491–506.
28. Shukla, R. D., Tripathi, R. K. Thakur, P. (2017) DC grid/bus tied DFIG based wind energy system .Renewable Energy, 108,179–193. 29.

29. Lalili, D., Berkouk, E. M., Boudjema, F. , Lourci, N. (2008) Self-Balancing of DC-link capacitor voltages using redundant vectors for SVPWM Controlled five-level Inverter, The Fifth International Multi-Conference on Systems, Signals Devices, IEEE SSD08, Amman, Jordan, paper reference, SSD08-15691–17326.
30. Boulkhrachef, S., Moualdia, A., Boudana, DJ. , Wira, P. (2019) Higher Order Sliding Mode Controler of a Wind Energy Conversion System, Nonlinear Dynamics and Systems Theory, **19** (04), 486–496.
31. Beltran1, B., Benbouzid, M.E.H., Ahmed-Ali, T. (2009) High-Order Sliding Mode Control of a DFIG-Based Wind Turbine for Power Maximization and Grid Fault Tolerance, IEEE International Electric Machines and Drives Conference, Miami,FL,USA, 183—189.

